SCIENCE CHINA Materials ARTICLES

mater.scichina.com link.springer.com

Published online 3 March 2021 | https://doi.org/10.1007/s40843-020-1594-2
*Sci China Mater* 2021, 64(6): 1449–1456

# Efficient control of emission and carrier polarity in $WS_2$ monolayer by indium doping

Ying Chen[1†], Ying Jiang[2†], Chen Yi[1], Huawei Liu[2], Shula Chen[1], Xingxia Sun[1], Chao Ma[1], Dong Li[1], Chenglin He[1], Ziyu Luo[1], Feng Jiang[2], Weihao Zheng[2], Biyuan Zheng[2], Boyi Xu[1], Zheyuan Xu[1] and Anlian Pan[1*]

**ABSTRACT** **Substitutional doping of two-dimensional (2D) transition metal dichalcogenides (TMDs) has been recognized as a promising strategy to tune their optoelectronic properties for a wide array of applications. However, controllable doping of TMDs remains a challenging issue due to the natural doping of these materials. Here, we demonstrate the controllable growth of indium-doped p-type $WS_2$ monolayers with various doping concentrations *via* chemical vapor deposition (CVD) of a host tungsten (W) source and indium (In) dopant. Scanning transmission electron microscopy confirmed that In atoms successfully substitute the W atoms in the $WS_2$ lattice. Intriguingly, the photoluminescence of the doped sample experiences strong intensity modulation by the doping concentration, which first increases remarkably with an enhancement factor up to ~35 and then decreases gradually when further increasing the doping concentration. Such a phenomenon is attributed to the progressive change of the exciton to trion ratio as well as the defect concentration in the doped samples. The assignment was further verified by the electric behavior of the fabricated In-doped $WS_2$ field effect transistors, which changes regularly from n-type to bipolar and finally to p-type behavior with increasing doping concentration. The successful growth of p-type monolayer $WS_2$ and the dual control of its optical and electrical properties by In doping may provide a promising method to engineer the opto-electronic properties of 2D materials.**

**Keywords:** controllable doping, chemical vapor deposition, photoluminescence intensity modulation, bipolar and p-type $WS_2$

## INTRODUCTION

Two-dimensional (2D) transition metal dichalcogenides (TMDs) have emerged as a versatile platform for nanoelectronics and optoelectronics [1–8]. In particular, doping investigation in these atomically thin layered materials has aroused great interest in recent years with the goal of enabling these materials for optical, electronic and optoelectronic applications [9–18]. Though doping of 2D TMDs can be achieved *via* intrinsic defects [19], substrate impurities [20], and molecular adsorption [21] or charge transfer [22], such approaches are typically not well controlled with poor stability, therefore limiting their practical uses in devices. An alternative strategy is employing substitutional doping of 2D TMDs to achieve more robust carrier type. However, substitutional doping encounters the same problem of losing the original optoelectronic properties of 2D TMDs, and the control of such doping to achieve desired optical and electric functionalities becomes challenging owing to the natural doping of the 2D materials.

For instance, electron-donating sulfur vacancies in $WS_2$ and $MoS_2$ monolayers are often present in large quantities during growth, making these 2D TMDs heavily n-doped in nature and thus difficult to achieve p-type conductivity. Pulsed laser deposition has been employed to achieve p-type conductivity in Nb-doped $WS_2$ bulk crystal [23], while there are limited reports on the direct growth of p-type monolayer TMDs by chemical vapor deposition (CVD). CVD is popular for manufacturing 2D materials because of its high level for controllable growth and large-scale production [24,25]. Several groups reported thermal CVD growth of Nb-doped monolayer $WS_2$ using solid powder sources, without the determination of carrier type after doping [14,18,26,27]. Only recently, liquid-mediated

[1] Department of Key Laboratory for Micro-Nano Physics and Technology of Hunan Province, State Key Laboratory of Chemo/Biosensing and Chemometrics, College of Materials Science and Engineering, Hunan University, Changsha 410082, China
[2] Department of School of Physics and Electronics, Hunan University, Changsha 410082, China
† These authors contributed equally to this work.
* Corresponding author (email: anlian.pan@hnu.edu.cn)

  

CVD growth was adopted to achieve p-type conductivity in Nb-doped monolayer $WS_2$ by liquid-phase precursor mixing [28]. Though substitutional doping to realize p-type 2D semiconductors was already demonstrated, more generalized doping strategy is highly desired to enrich such studies for versatile functions and especially to get deep insights into the doping mechanism that usually involves complex optical properties. Moreover, present reports on achieving p-type conductivity by CVD growth mainly focus on vanadium [29], niobium [14,18,26,27,28] and phosphorus [30]. Indium (In)-doped p-type conductivity regulation has not yet been explored.

Here, we report the successful growth of In-doped monolayer $WS_2$ by using atmospheric pressure one-step CVD growth method. The controllable doping of $WS_2$ is realized by adjusting the weight ratio of the precursor ($In_2O_3$, $WO_3$). High-angle annular dark field scanning transmission electron microscopy (HAADF-STEM) confirms that In atoms successfully substitute the W atoms across the whole $WS_2$ flake. Optical measurements show that the photoluminescence (PL) of the doped sample is significantly enhanced when the weight ratio of the precursor ($In_2O_3$, $WO_3$) is 1:8, with an enhancement factor up to ~35 compared with that of undoped $WS_2$. Subsequently, the PL intensity progressively decreases and eventually resembles that in the undoped sample, as the weight ratio increases from 1:5 to 1:3. On the other hand, electrical measurements demonstrate that In-doped $WS_2$ field effect transistors (FET) feature room-temperature transfer characteristics changing from n-type to bipolar and finally to p-type as the concentration of $In_2O_3$ increases, implying the transition from electron doping to hole doping of the monolayer $WS_2$ by increasing the doping concentration. The mechanism of dual regulation of the optical and electrical properties is ascribed to the gradual change of both the exciton to trion ratio and the defect concentration by In doping. Our results provide a facile and convenient method to achieve controllable doping in 2D TMDs, which allows for efficient tuning of both optical and electrical properties towards excellent optoelectric device performance.

## EXPERIMENTAL SECTION

### Materials synthesis

The In-doped $WS_2$ monolayers were synthesized by a typical one-step CVD growth method. The mixed powder of NaCl and metal oxide precursors ($In_2O_3$ ($x$ mg, $x$ = 3.75, 6, 10) and $WO_3$ (30 mg)) was selected as the solid source for the one-step growth. For In-doped $WS_2$ monolayers, the boat with precursor ($WO_3$ and $In_2O_3$) (99.9%, Alfa Aesar) was put at the center of the furnace. Then, the $SiO_2$/Si substrate was placed at the backward position about 2 cm away from the precursor ($WO_3$ and $In_2O_3$), and the sulfur powder (99.9%, Alfa Aesar) was placed 12 cm upstream from the furnace center. Before heating, the system was cleaned by injecting 800 sccm argon gas and maintained for about 15 min. The temperature was gradually heated up to 800°C for 18 min, and then kept at 800°C for 5 min. Meanwhile, the sulfur powder was put in the upstream region with temperature at 200°C. The gas flow of 90 sccm argon was used as the carrier gas. After growth, the furnace was cooled down to room temperature naturally.

### Characterizations

The morphologies and structure information of the samples were characterized by an optical microscope (Zeiss Axio Scope A1), a scanning electron microscope (SEM, ZEISS. Sigma HD), an atomic force microscope (AFM, Bruker Multimode 8), and a transmission electron microscope (TEM, Tecnai G2 F20 S-TWIN) combined with energy dispersive X-ray spectroscopy (EDS). Raman and PL measurements were conducted using a confocal microscope (WITec, alpha-300). The electrical and optoelectronic properties of the as-fabricated devices were performed in a vacuum Lake Shore Probe Station combined with an Agilent B1500A semiconductor analyzer at room temperature. For STEM measurements, the nanosheets were transferred onto copper grid using a poly (methyl methacrylate) (PMMA, $M$w = 950k, 4 wt%, AR-P679.04, All resist)-mediated nano transfer method (speed: 4000 rpm, 30 s). Then the edge of the baked wafer was round up with scotch tape, and subsequently immersed into the KOH (15 mol $L^{-1}$) solution for 12 h. Then the PMMA film was taken out from the KOH solution and flushed with deionized (DI) water. The cleaned PMMA film was removed onto a grid of copper in the atmosphere of acetone vapor at 30°C. Finally, the PMMA film was taken away by acetone vapor, leaving the doped 2D TMDCs sample on the grid of copper. The STEM measurements were carried out on a JEOL ARM200F microscope operated at 200 kV and equipped with a probe-forming aberration corrector. For HAADF-STEM images, the inner and outer collection angles of the ADF detector were 68 and 280 mrad, respectively, and the convergence semiangle was about 28 mard. Time-resolved PL (TRPL) experiments were performed using a confocal microscope (WITec, alpha-300) as the collection device, and the emission signal was reflected into a streak

  

camera (C10910, Hamamatsu) by Ag mirrors. Ti:sapphire laser pulses at 400 nm (with a repetition rate of 80 MHz and a pulse width of 80 fs) were used as the light source. The 400-nm output was generated by passing an 800-nm laser beam from a mode-locked oscillator (Tsunami 3941-X1BB, SpectraPhysics) through a BBO crystal. The 400-nm laser beam was then focused onto the sample with a spot diameter of ~3 μm from the top by an objective lens (50×, Zeiss, 0.75 NA).

**Device fabrication and measurement**

A layer of PMMA (495 K, A4, Microchem Company) was spin-coated on the $SiO_2$ (300 nm)/Si substrate with prepared materials and subsequently baked for 5 min at 170°C on the hot plate. The drain-source electrodes were defined by electron beam lithography (Raith 150 two) and were composed of Cr/Au (10 nm/50 nm) by thermal evaporation, finally followed by lift-off process with acetone. The electrical properties of the devices were measured in vacuum Lake Shore Probe Station and Agilent B1500A semiconductor analyzer at room temperature.

## RESULTS AND DISCUSSION

The controllable synthesis of indium-doped monolayer $WS_2$ (In:$WS_2$) was carried out through the one-step CVD growth method, as shown in Fig. 1a, b. During the process of indium doping in $WS_2$, a small amount of indium atoms replaced the positions of W atoms when $WS_2$ crystals were formed. Growth precursors were prepared by stirring various amounts of NaCl and metal oxide precursors ($In_2O_3$ and $WO_3$). After a homogeneous powder obtained, the powder was evenly drop-casted on a porcelain boat, and the sulfur vapor reaction was performed at 800°C with argon as the carrier gas, as shown in Fig. 1a. In this experiment, we controlled the doping concentration by varying the weight ratio of the precursors $In_2O_3$ and $WO_3$. The ratio of $In_2O_3$ to $WO_3$ mentioned in the following text represents the dosage and weight ratio of powder. Fig. 1c shows the optical microscopy image of heavily doped samples with a ratio of 1:3. Optical microscopy images of other doped samples show the crystallites with similar size, morphology, and optical contrast (Fig. S1). The SEM image reveals that a typical growth process results in micrometer-sized triangular islands (Fig. 1d). Fig. 1e shows the AFM image of the doped sample with a ratio of 1:3. The line profile reveals that the step height at the $WS_2$ edge is around 0.96 nm after doping, indicating that the sample is still a monolayer with uniform thickness distribution rather than heterojunction.

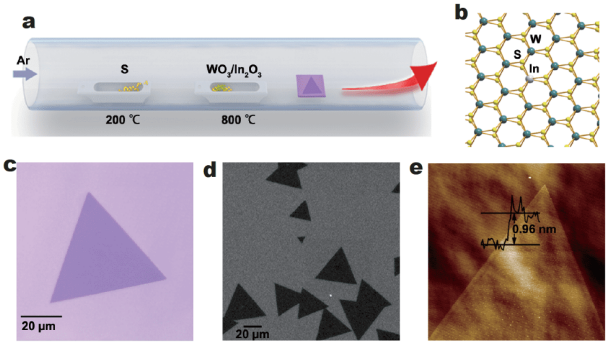


**Figure 1** (a, b) Schematic diagram of synthesis process and atomic configuration of the In:$WS_2$. (c) Optical image of the as-prepared In:$WS_2$ on the Si/$SiO_2$ substrate. (d) SEM and (e) AFM images of the In:$WS_2$. All the characterized samples were prepared with the precursor ratio ($In_2O_3$:$WO_3$) of 1:3.

Fig. 2a shows the high-resolution TEM (HR-TEM) image of the doped sample with the precursor ratio of 1:3, indicating that the layered structure is preserved when In ions are doped in $WS_2$. The fast Fourier transform pattern in the inset of Fig. 2a confirms the crystal structure and crystallinity of the doped sample. The EDS spectra display the existence of In-concentration of 1.69, 3.48 and 6.04 at%, respectively, in the 1:8, 1:5, and 1:3 doped samples (Fig. S2). To identify the location of In dopant within $WS_2$, the doped samples were further characterized by HAADF-STEM (Fig. 2b). Since the HAADF intensity is proportional to atomic numbers ($Z$) and the $Z$ in S ($Z$ = 16), W ($Z$ = 74) and In ($Z$ = 49) are different, those atoms marked in the yellow circles can be found in Fig. 2b. Fig. 2c is an expanded view of the red area in Fig. 2b, showing that there is a significant difference in the atomic brightness between the central part and the surrounding area. Fig. 2d is the simulation calculation diagram of Fig. 2c and it also verifies the difference in atomic brightness of the two areas. Fig. 2e is the intensity spectra of the selected area of Fig. 2d, where W atoms show stronger intensity compared with In atoms. The HAADF-STEM images of the doped samples with different precursor ratios show that the number of In atoms increases as the ratio of the precursor increases in the doped samples (Fig. S3). The experimental results from HAADF-STEM confirm that In atoms successfully replace the W atoms. Fig. 2f–h show the X-ray photoelectron spectroscopy (XPS) results from the CVD grown undoped $WS_2$ and In:$WS_2$ (1:3). Fig. 2f, g show the binding energies of W 4f and S 2p core levels, respectively. These peaks of S $2p_{1/2}$ (164.1 eV), S $2p_{3/2}$ (163.0 eV), W $4f_{5/2}$ (35.5 eV) and W $4f_{7/2}$ (33.4 eV) core

  

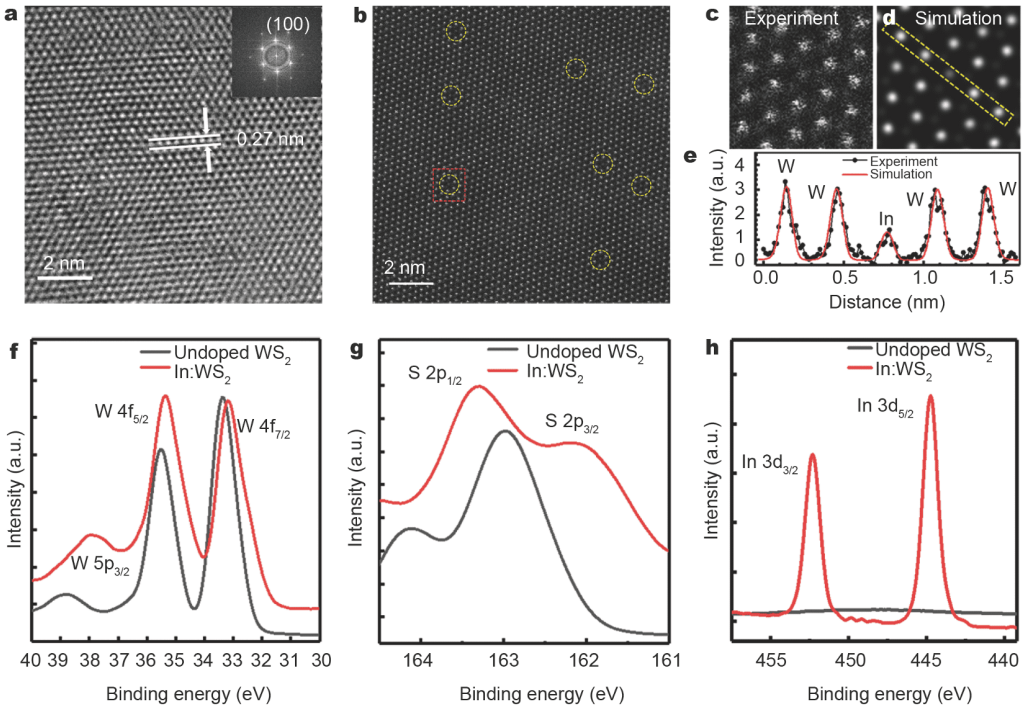


**Figure 2** (a) HR-TEM image of the In:$WS_2$ with monolayer edges. The inset in (a) shows the corresponding electron diffraction patterns. (b) HAADF-STEM image of the prepared In:$WS_2$ sample. (c) Expanded figure of the red area in (b). (d) Simulation figure of (c). The In atom can be identified from (e) intensity spectra of the selected area where W atoms show stronger intensity compared with that of In atoms. XPS scans of (f) W 4f, W 5p, (g) S 2p, and (h) In 3d core-levels measured from undoped $WS_2$ and In:$WS_2$ samples. All samples were prepared with the precursor ratio ($In_2O_3$:$WO_3$) of 1:3.

levels are assigned to the undoped $WS_2$. In the In-doped $WS_2$ sample, both S 2p and W 4f levels shift toward lower binding energy by 0.9 and 0.2 eV, respectively. This indicates that the Fermi level of the In-doped $WS_2$ shifts toward the valence band, which is consistent with the expected acceptor behavior of In dopants. This lowering of the Fermi level indicates that In substitutional impurities introduce p-type doping in the $WS_2$ monolayer, which is explained by the fact that In possesses three less valence electrons as compared with W. As expected, the distinct binding energy peaks corresponding to In 3d core-levels at 444.7 and 452.3 eV were detected only in the In:$WS_2$ sample (Fig. 2h). This phenomenon implies that the incorporation of In into the $WS_2$ lattices essentially preserves the $In^{3+}$ state. Both the STEM and XPS results provide clear evidences that In atoms are incorporated into $WS_2$ lattice *via* substitution cation doping rather than surface adsorption or decoration.

In the following, the optical properties of undoped and In-doped monolayer $WS_2$ were examined. Fig. 3a–d show the PL intensity maps of the undoped and In-doped samples. It can be seen that when the precursor ratio ($In_2O_3$:$WO_3$) is 1:8, the PL intensity is remarkably enhanced, and the enhancement factor can be up to ~35 (Fig. S4). As the doping concentration further increases (1:5), the PL intensity turns to decrease, and when the precursor ratio reaches 1:3, the PL intensity decays to be equivalent to or even lower than that of the undoped sample. Fig. 3e, f respectively show the PL spectra of the edge and the central areas of the triangular monolayers shown in Fig. 3a–d, demonstrating that the emission intensity of these two areas have the same evolution trend with the doping concentration. Together with the results from STEM and XPS characterization, such an unusual PL intensity modulation very likely arises from the progressive change of the exciton to trion ratio as well as the defect concentration in the sample by In doping. When the doping concentration is low (1:8), the significantly enhanced PL intensity can be attributed to the p-type doping of In neutralizing the excess electrons in $WS_2$, resulting in the increase of exciton density *via* the transformation of negative trions ($X^-$) to neutual excitons ($X^0$). In addition, this p-type doping could also weaken the electrostatic screening and the many-body effect in $WS_2$ monolayer, leading to a further enhanced PL emission. When the doping concentration increases further,

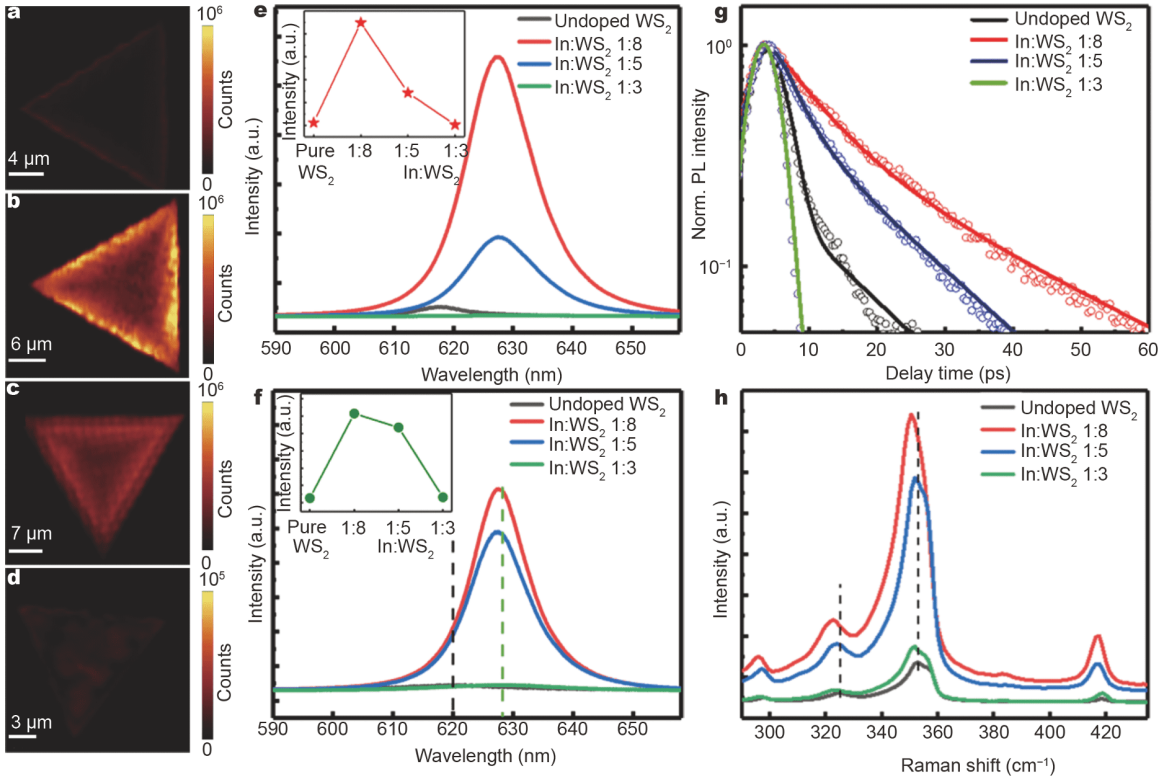


**Figure 3** Spatially resolved PL intensity maps of undoped $WS_2$ (a) and In:$WS_2$ with the precursor proportion of (b) 1:8, (c) 1:5 and (d) 1:3. The PL spectra of the edge and center regions of the triangular monolayers in (a–d) are shown in (e) and (f), respectively. The insets in (e) and (f) are the corresponding trend graphs of the PL spectral integral areas of the undoped $WS_2$ and In:$WS_2$ samples. TRPL dynamics and Raman spectra of the undoped $WS_2$ and In:$WS_2$ with different precursor proportions (1:8, 1:5 and 1:3) are shown in (g) and (h), respectively.

extra positive charges will be introduced and a transition from $X^0$ to positive trions ($X^+$) will take place, turning to decrease the PL intensity with the doping concentration. With a precursor ratio of 1:3, the PL intensity decays to resemble or even be lower than that of the undoped $WS_2$, and positive trions ($X^+$) should be the dominant species in this case, as evidenced in latter electrical characterizations. Component decomposition of the PL spectra reveals the spectral distribution of the neutral ($X^0$) and charged ($X^T$, $T$ = "–" or "+") species, with $X^T$ slightly redshifts (Fig. S5). The ratio of $X^0$ and $X^T$ intensity increases first and then decreases with the increase of doping concentration, which verifies the above hypothesis. The broad linewidths of the spectral components, especially for $X^T$, imply the involvement of defects in modulating the PL emission to lower its intensity in all samples. The broadest linewidth in the case with a precursor ratio of 1:3 indicates the more extra defects introduced by the intensively p-type doping, part of the reason for its very weak PL intensity even lower than that of the undoped sample (in addition to the contribution from $X^+$ species).

Moreover, the TRPL measurements further confirm the previous proposal for PL intensity modulation by p-type doping. Decay curves of the four samples were integrated over the emission peak and summarized in Fig. 3g. As expected, the decay profile of the doped sample is first greatly elongated with respect to that of undoped sample and then it turns to be progressively shortened when further increasing the doping concentration. By fitting the decay curves, two lifetime components are obtained (Table S1 and Fig. S6), where the fast component on the order of sub-picosecond to several picoseconds is generally ascribed to the relaxation of trion species while the slow component on tens of picoseconds is assigned to that of neutual exciton species [31,32]. As seen, both the ratio of exciton to trion components and the lifetime values first increase and then decrease gradually with the doping concentration, with the average lifetime in the trend of 1:8 > 1:5 > undoped $WS_2$ > 1:3, which matches very well with the PL intensity behavior and thus strongly supports the proposed mechanism for PL intensity modulation by In doping. The PL spectrum of the doped

  

sample slightly red-shifts compared with the undoped sample, which may be caused by strain and doping. This difference can be further verified by the Raman spectrum in Fig. 3h. The Raman peaks of all In-doped samples red shift 2 $cm^{-1}$, which indicates the possible influences of In doping, defects and strain engineering on the 2D $WS_2$ electronic structure.

The electrical properties of both the In-doped and undoped $WS_2$ samples were further investigated *via* fabricating bottom-gated FETs based on these samples. Electrostatic gating is achieved using heavily doped Si as the back gate electrode, which shows the output (drain–source current ($I_{ds}$) *vs.* drain-source voltage ($V_{ds}$)) and transfer ($I_{ds}$ *vs.* gate bias ($V_{gs}$) ) characteristics of the undoped and doped monolayer $WS_2$. The transfer characteristics of the undoped sample that turns on at $V_{gs}$ ~ −40 V (Fig. 4b) is similar to previously reported results, implying its strong n-type character. When the weight ratio of precursor $In_2O_3$:$WO_3$ is larger than 1:8, hole branch appears at large negative gate biases (Fig. 4c, d). With In-doping increasing (1:5), a bipolar electrical transfer curve appears (Fig. 4f). It is worth noting that when the weight ratio of the precursor $In_2O_3$:$WO_3$ is larger than 1:3 (Fig. 4h), it presents a completely p-type

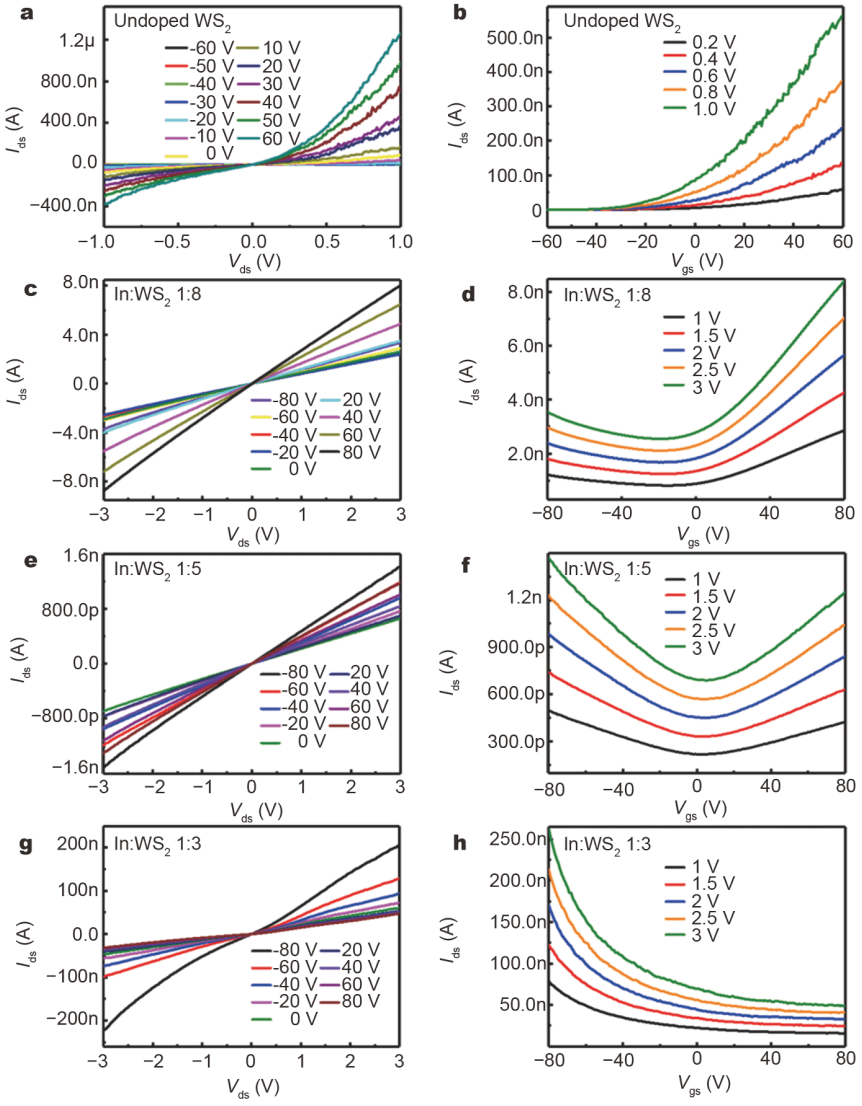


**Figure 4** Electrical transport properties of four FETs based on the undoped and In-doped monolayers $WS_2$. The left columns (a, c, e and g) show the output characteristics ($I_{ds}$ *vs.* $V_{ds}$). The right columns (b, d, f and h) show the transfer behaviors ($I_{ds}$ *vs.* $V_{gs}$) in different In-doped concentrations. The undoped monolayer (b) is highly n-type conductive. With the In-doped concentration increasing, the monolayer exhibits excellent p-type conduction mode (h).

$WS_2$ semiconductor, implying that sufficient electron acceptors are provided in the heavy doping of indium. This n- to p-type transition of the electrical behavior gives a direct evidence that In dopants can act as electron acceptors to effectively compensate the natural n-type dopants in pristine $WS_2$. The changed trend of the electrical properties is consistent with the previous optical test, which further proves the previous proposed mechanism that the exciton to trion ratio in $WS_2$ system is progressively changed with the dominant species transition from negative trions ($X^-$) to finally positive trions ($X^+$) as the In doping concentration increases. The doping of dual control of optics and electricity are rarely reported previously, and is expected to have potential applications in the fields of electronics and optoelectronics.

## CONCLUSIONS

In summary, we have demonstrated the successful growth of In-doped monolayer $WS_2$ with various doping concentrations. Our growth method is a one-step process using simple and feasible CVD growth in which impurities with host material precursor were doped. Controlling the doping concentration by adjusting the weight ratio of the precursor ($In_2O_3$, $WO_3$), the growth products are relatively stable. In addition, by changing the doping concentration, both the optical and electrical properties of the doping system can be regularly modulated, and either PL intensity enhancement or bipolar/p-type $WS_2$ monolayers can be achieved by appropriate In doping. This controllable dual tuning of the material properties by In doping may provide a promising method to engineer the electronic structures of 2D TMDs and thus expand their applications in versatile optoelectronic devices.

**Received 26 October 2020; accepted 22 December 2020; published online 3 March 2021**


1 Mak KF, Shan J. Photonics and optoelectronics of 2D semiconductor transition metal dichalcogenides. Nat Photon, 2016, 10: 216–226
2 Duan X, Wang C, Pan A, *et al.* Two-dimensional transition metal dichalcogenides as atomically thin semiconductors: Opportunities and challenges. Chem Soc Rev, 2015, 44: 8859–8876
3 Lopez-Sanchez O, Lembke D, Kayci M, *et al.* Ultrasensitive photodetectors based on monolayer $MoS_2$. Nat Nanotech, 2013, 8: 497–501
4 Li F, Feng Y, Li Z, *et al.* Rational kinetics control toward universal growth of 2D vertically stacked heterostructures. Adv Mater, 2019, 31: 1901351
5 Withers F, Del Pozo-Zamudio O, Mishchenko A, *et al.* Light-emitting diodes by band-structure engineering in van der Waals heterostructures. Nat Mater, 2015, 14: 301–306
6 Qiu DY, da Jornada FH, Louie SG. Optical spectrum of $MoS_2$: Many-body effects and diversity of exciton states. Phys Rev Lett, 2013, 111: 216805
7 Duan X, Wang C, Shaw JC, *et al.* Lateral epitaxial growth of two-dimensional layered semiconductor heterojunctions. Nat Nanotech, 2014, 9: 1024–1030
8 Mak KF, Lee C, Hone J, *et al.* Atomically thin $MoS_2$: A new direct-gap semiconductor. Phys Rev Lett, 2010, 105: 136805
9 Resta GV, Balaji Y, Lin D, *et al.* Doping-free complementary logic gates enabled by two-dimensional polarity-controllable transistors. ACS Nano, 2018, 12: 7039–7047
10 Bai G, Yuan S, Zhao Y, *et al.* 2D layered materials of rare-earth Er-doped $MoS_2$ with NIR-to-NIR down- and up-conversion photoluminescence. Adv Mater, 2016, 28: 7472–7477
11 Zhao Y, Xu K, Pan F, *et al.* Doping, contact and interface engineering of two-dimensional layered transition metal dichalcogenides transistors. Adv Funct Mater, 2017, 27: 1603484
12 Kochat V, Apte A, Hachtel JA, *et al.* Re doping in 2D transition metal dichalcogenides as a new route to tailor structural phases and induced magnetism. Adv Mater, 2017, 29: 1703754
13 Chang RJ, Sheng Y, Ryu GH, *et al.* Postgrowth substitutional tin doping of 2D $WS_2$ crystals using chemical vapor deposition. ACS Appl Mater Interfaces, 2019, 11: 24279–24288
14 Gao J, Kim YD, Liang L, *et al.* Transition-metal substitution doping in synthetic atomically thin semiconductors. Adv Mater, 2016, 28: 9735–9743
15 Lin YC, Dumcenco DO, Komsa HP, *et al.* Properties of individual dopant atoms in single-layer $MoS_2$: Atomic structure, migration, and enhanced reactivity. Adv Mater, 2014, 26: 2857–2861
16 Suh J, Park TE, Lin DY, *et al.* Doping against the native propensity of $MoS_2$: Degenerate hole doping by cation substitution. Nano Lett, 2014, 14: 6976–6982
17 Suh J, Tan TL, Zhao W, *et al.* Reconfiguring crystal and electronic structures of $MoS_2$ by substitutional doping. Nat Commun, 2018, 9: 199
18 Gao H, Suh J, Cao MC, *et al.* Tuning electrical conductance of $MoS_2$ monolayers through substitutional doping. Nano Lett, 2020, 20: 4095–4101
19 Chow PK, Jacobs-Gedrim RB, Gao J, *et al.* Defect-induced photoluminescence in monolayer semiconducting transition metal dichalcogenides. ACS Nano, 2015, 9: 1520–1527
20 Cui X, Lee GH, Kim YD, *et al.* Multi-terminal transport measurements of $MoS_2$ using a van der waals heterostructure device platform. Nat Nanotech, 2015, 10: 534–540
21 Mouri S, Miyauchi Y, Matsuda K. Tunable photoluminescence of monolayer $MoS_2$ *via* chemical doping. Nano Lett, 2013, 13: 5944–5948
22 Kiriya D, Tosun M, Zhao P, *et al.* Air-stable surface charge transfer doping of $MoS_2$ by benzyl viologen. J Am Chem Soc, 2014, 136: 7853–7856
23 Rathod UP, Egede J, Voevodin AA, *et al.* Extrinsic p-type doping of few layered $WS_2$ films with niobium by pulsed laser deposition. Appl Phys Lett, 2018, 113: 062106
24 Gong C, Hu K, Wang X, *et al.* 2D nanomaterial arrays for electronics and optoelectronics. Adv Funct Mater, 2018, 28: 1706559
25 Zhou J, Lin J, Huang X, *et al.* A library of atomically thin metal chalcogenides. Nature, 2018, 556: 355–359
26 Sasaki S, Kobayashi Y, Liu Z, *et al.* Growth and optical properties of Nb-doped $WS_2$ monolayers. Appl Phys Express, 2016, 9: 071201
27 Jin Y, Zeng Z, Xu Z, *et al.* Synthesis and transport properties of degenerate p-type Nb-doped $WS_2$ monolayers. Chem Mater, 2019,


  

31: 3534–3541
28 Qin Z, Loh L, Wang J, *et al.* Growth of Nb-doped monolayer $WS_2$ by liquid-phase precursor mixing. ACS Nano, 2019, 13: 10768–10775
29 Zhang L, Wang G, Zhang Y, *et al.* Tuning electrical conductance in bilayer $MoS_2$ through defect-mediated interlayer chemical bonding. ACS Nano, 2020, 14: 10265–10275
30 Lee JS, Park CS, Kim TY, *et al.* Characteristics of p-type conduction in P-doped $MoS_2$ by phosphorous pentoxide during chemical vapor deposition. Nanomaterials, 2019, 9: 1278
31 Fan P, Zheng B, Sun X, *et al.* Trion-induced distinct transient behavior and stokes shift in $WS_2$ monolayers. J Phys Chem Lett, 2019, 10: 3763–3772
32 Fan X, Zheng W, Liu H, *et al.* Nonlinear photoluminescence in monolayer $WS_2$: parabolic emission and excitation fluence-dependent recombination dynamics. Nanoscale, 2017, 9: 7235–7241

**Acknowledgements** This work was financially supported by the National Natural Science Foundation of China (51525202, 61635001, 52072117 and 21703059), the Key Program of the Hunan Provincial Science and Technology Department (2019XK2001), and the International Science and Technology Innovation Cooperation Base of Hunan Province (2018WK4004).

**Author contributions** Chen Y, Jiang Y and Pan A conceived and designed the project, and wrote the manuscript. Liu H, Sun X and Li D performed the device fabrication and characterizations. Yi C, Ma C, Chen S, He C, Luo Z, Jiang F, Zheng W, Zheng B, Xu B and Xu Z conducted the SEM, STEM, AFM, PL, TRPL and Raman measurements, and advised on data analysis. Pan A supervised the experiments and provided theoretical guidance. All authors contributed to the general discussion.

**Conflict of interest** The authors declare no conflict of interest.

**Supplementary information** Supporting data are available in the online version of the paper.

**Ying Chen** is currently a PhD candidate at the College of Materials Science and Engineering, Hunan University. His main research interests include the synthesis of nanomaterials with controlled CVD route, and their applications in photoelectric devices.

**Ying Jiang** received her MSc degree in electronics and systems from Jilin University in 2010 and PhD degree ("Pass with Distinction and Honour") in physical chemistry from Instituto Superior Tecnico, University of Lisbon, in 2015. She is currently an associate professor at the School of Physics and Electronics, Hunan University. Her current research interests focus on the ultrafast spectroscopic study of 2D transition metal dichalcogenide materials and perovskite nanostructures.

**Anlian Pan** received his PhD degree from the Institute of Physics, Chinese Academy of Sciences in 2006. Afterwards, he worked for one year as a Humboldt Research Fellow with Prof. Ulrich Goesele at the Max Planck Institute of Microstructure Physics, and then joined Arizona State University as a Postdoctoral Fellow, where he became a research assistant professor. He joined Hunan University in 2010 and has been working as the distinguished professor of "Furong Scholar" in Hunan province since then. His research interests include the micro-nano optical, electronics of semiconductor nanostructures.

## 通过铟掺杂有效控制单层$WS_2$的发射和载流子极性

陈荧[1†], 蒋英[2†], 易琛[1], 刘华伟[2], 陈舒拉[1], 孙兴霞[1], 马超[1], 李东[1], 何承林[1], 骆子煜[1], 姜峰[2], 郑玮豪[2], 郑弼元[2], 徐博一[1], 徐哲元[1], 潘安练[1*]

**摘要** 二维(2D)过渡金属硫族化合物(TMDs)的掺杂被认为是调控其光电特性的一种有效途径. 但是TMDs材料在制备过程中会引入自身掺杂, 使其可控掺杂仍具有较大的挑战. 本文中我们通过含有钨(W)源和铟(In)源掺杂剂的化学气相沉积法(CVD)实现了不同铟掺杂浓度的单层$WS_2$的可控制备. 扫描透射电镜结果表明In原子成功取代了$WS_2$晶体中的W原子. 掺杂样品的发光特性受到了In掺杂浓度的明显调制, 其发光强度随掺杂浓度呈现出先增强后衰减的趋势, 最大增强倍数可达约35倍. 这一现象主要归因于In掺杂后$WS_2$体系中激子与三激子的比例随掺杂浓度逐渐变化. 基于In掺杂的$WS_2$场效应晶体管的电学特性表明, 随着In掺杂浓度的增加, 单层$WS_2$实现了从本征n型到双极性, 最终到p型半导体的转变, 表明掺杂样品的载流子极性也受到了掺杂浓度的有效调控. 通过In掺杂可实现p型单层$WS_2$的成功制备, 并且可对$WS_2$体系光学和电学特性进行双重调制, 为实现2D材料光电特性的有效调控提供了一种潜在的可行方法.

  